Chapter 5

Photocatalytic property assessment of recovered high added-value materials

5. Photocatalytic property assessment of recovered high added-value materials

5.1. Introduction to wastewater generation and treatment

In textile manufacturing industries, textile made from synthetic or natural fibers are sized, scoured, bleached, mercerized, dyed, printed and finished to obtain a variety of products (Kishor et al., 2021). Textile industries drive global economies in countries like China, India, Pakistan, Brazil, Bangladesh, and Malaysia but also significantly contribute to environmental pollution. They consume massive amounts of water and synthetic chemicals, generating coloured wastewater with hazardous pollutants that often end up in rivers and seas. For instance, in India's Kanpur city, textile waste flows into the Ganga River. In India, approximately 830 million m^3/year of groundwater is used, with around 640 million m^3/year discharged as wastewater (Jegatheesan et al., 2016). Dye loaded wastewater from these industries pose risks to both the environment and human health, if not properly managed. It causes eutrophication and disturbs aquatic life, causes groundwater and soil pollution. When this wastewater is used in crop irrigation, the contaminants accumulate in the food chain. Such effluent discharge is toxic in nature and may cause cancer, low sperm mobility, eye and skin irritation, hence adversely affecting human health (Azanaw et al., 2022). So wastewater treatment is necessary to control water pollution, avoid the shortage of clean and safe water, and ensure its sustainable utilization. *Figure 5.1* offers an overview of wastewater generation stages, their impact, and treatment approaches.

Several effluent treatment methods have been reported. Physical methods involving settling, skimming; chemical-induced precipitation, disinfection, and biological methods involving introduction of micro-organisms have been reported in the past to treat wastewater. The integration of physical, chemical, and biological methods in combined treatment approaches leads to improved degradation and mineralization of textile dyes and

wastewater from textile industries compared to individual methods used alone. These methods are costly and do not involve destruction of pollutant substances. So radiation-assisted advanced wastewater treatment process such as heterogeneous photocatalysis has been utilized. Here wastewater is treated in the presence of semiconductor photocatalyst. Photocatalysis is easy to apply, less costly, can proceed at ambient conditions, and environment friendly. It involves the elimination of pollutants rather than transferring them from one phase to another (Kishor et al., 2021).

In their study, Anani et al. discovered that nanomaterials are effective tools for sustainable water purification. These materials possess advantageous characteristics such as small pore size, high porosity, commercial incentives, strong adhesion, and excellent absorption properties. These properties enable them to efficiently eliminate inorganic and organic solutes, harmful metals, emerging pollutants, and microbes from both wastewater and drinking water, all without generating additional pollutants (Anani et al., 2023).

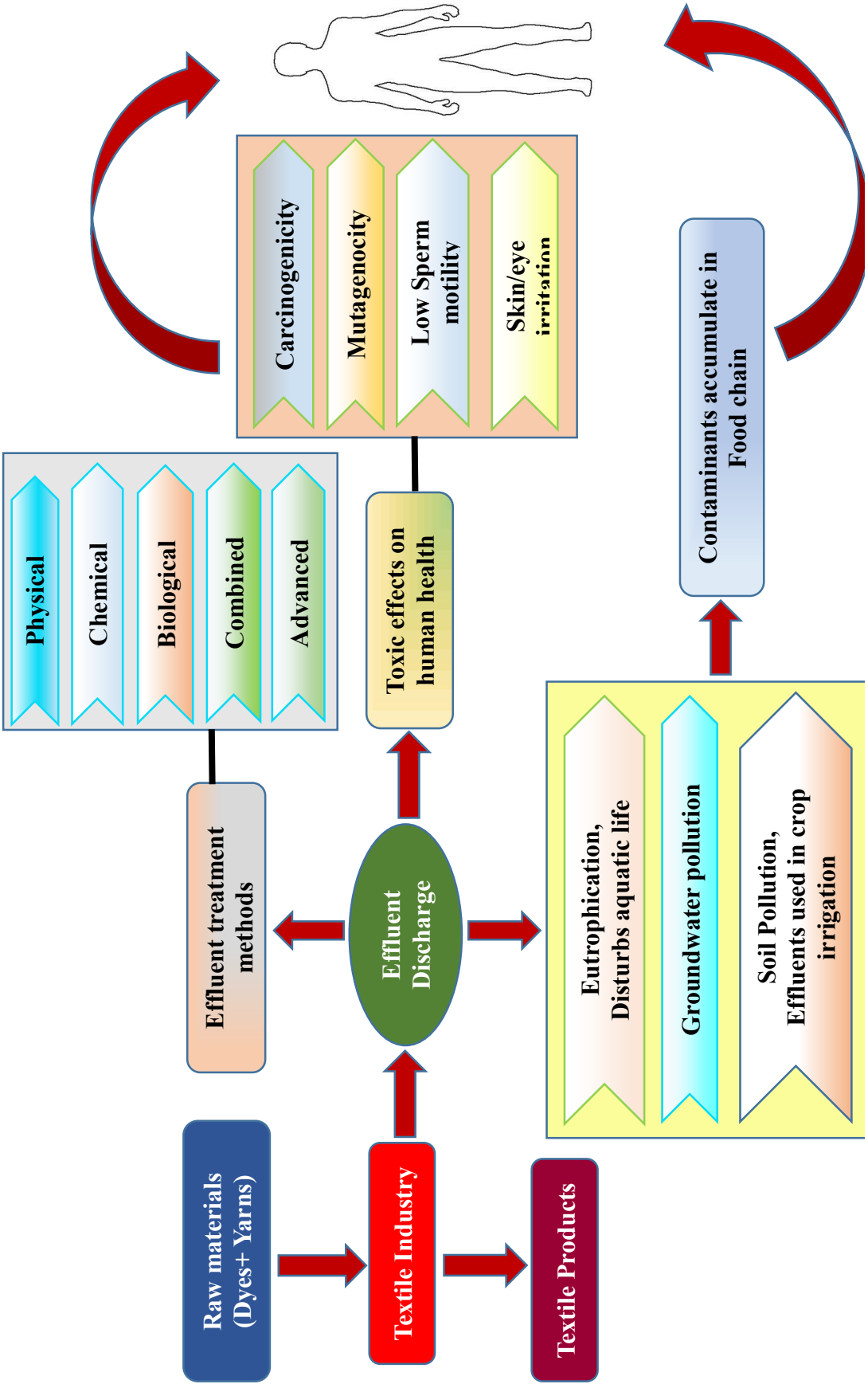

Figure 5.1 Wastewater generation, its toxicity and treatment approaches in textile industry (modified from Azanaw et al., 2022)

5.2. Photocatalysis

Photocatalysis utilizes a semiconductor catalyst capable of capturing sunlight photons and generating electron-hole pairs, which assist in breaking down organic dyes using a safe and eco-friendly approach (Dong et al., 2015). Utilizing catalysts that can effectively absorb visible light while also meeting various practical requirements such as versatility, affordability, recyclability, and ease of fabrication is crucial. With their narrow energy gaps, cuprous oxide (Cu_2O), cupric oxide (CuO), and copper hydroxide ($Cu(OH)_2$) emerge as promising contenders for these reasons (Meyer et al., 2012).

The photocatalytic mechanism of degradation of organic pollutants in presence of sunlight is shown in *Figure 5.2*. On visible light irradiation, the photocatalytic material absorbs energy of light and causes electrons to move from valence band to the conduction band, leaving behind holes in the valence band (as shown in *Eq. 5.1*). These photogenerated electrons reduce the oxygen molecule present in the reaction system (*Eq. 5.4*). The holes oxidize adsorbed water molecules (*Eq. 5.2 & 5.3*). As a result of this reduction-oxidation, superoxide radical ($O_2^{-\cdot}$) and hydroxyl radical ($OH^{\cdot}$) are formed, which act as reactive species to breakdown the dye molecules to form CO_2, H_2O, and other less harmful by-products (*Eq. 5.5*). Without electron-hole scavengers, the electron-hole pairs produced by light absorption may recombine within few nanoseconds and least or no dye degradation would be observed. Oxygen vacancies act as electron acceptors during the photocatalytic reaction and thus reduce the recombination rate. Oxygen vacancies also facilitate the adsorbed oxygen to capture photo-induced electrons and generate superoxide radicals, hence enhancing the photocatalytic property (Gautam et al., 2023b, 2023a).

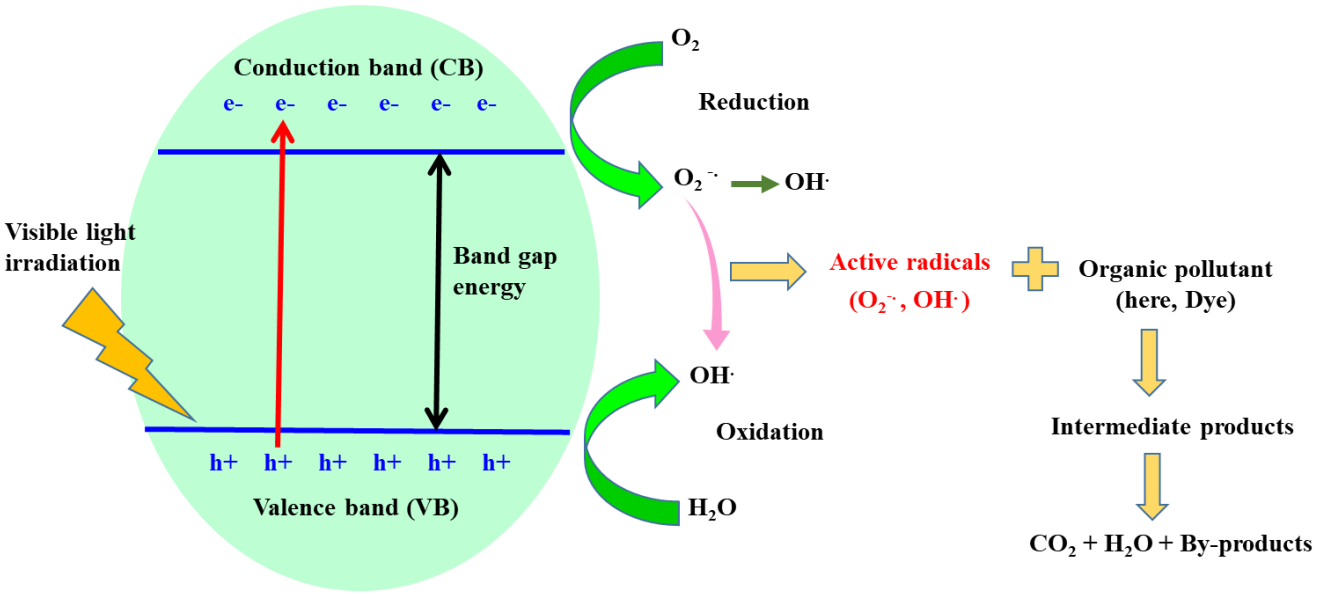

Figure 5.2 Photocatalytic mechanism of organic pollutant degradation in presence of photocatalyst

$$CuO + h\nu \rightarrow h^{+}_{VB} + e^{-}_{CB} \quad (5.1)$$

$$h^{+}_{VB} + H_2O \rightarrow \cdot OH + H^{+} \quad (5.2)$$

$$h^{+}_{VB} + OH^{-}_{(ads)} \rightarrow \cdot OH \text{ (hydroxyl)} \quad (5.3)$$

$$e^{-}_{CB} + O_{2\,(ads)} \rightarrow O_2^{\cdot -} \text{ (superoxide)} \quad (5.4)$$

$$\text{Dye} + O_2^{\cdot -}/\cdot OH \rightarrow \text{Degradation product } (H_2O + CO_2 + \text{By-products}) \quad (5.5)$$

In this section the nanoproducts synthesized in previous chapter are explored of their photocatalytic activity by studying the degradation of textile dyes Congo Red (CR) and Methylene Blue (MB).

5.3. Degradation of Congo Red

Congo red is an azo dye commonly found in textile industries effluents. It is carcinogenic, toxic, and harmful in nature. So the effluent needs an effective treatment and elimination before it enters into the environment (Maheo et al., 2022). Its chemical structure is given in *Figure 5.3*. It has maximum absorption peak at 497 nm wavelength (Gautam et al., 2023a).

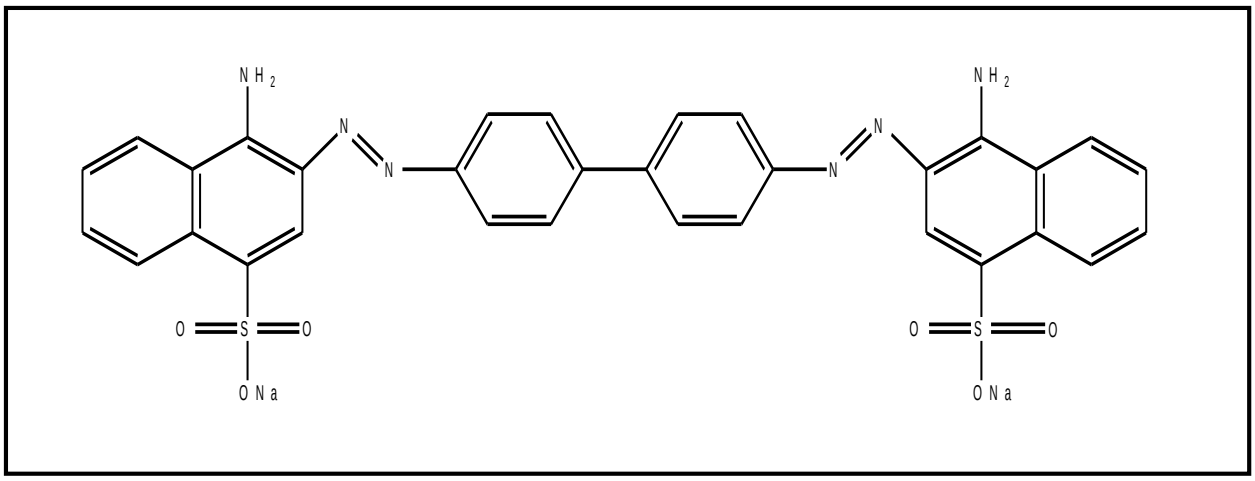

Figure 5.3 Chemical structure of Congo red

5.3.1. Photocatalytic activity assessment

In a 4 ml quartz cuvette, a solution was prepared by mixing 1 ml of distilled water, 1 ml of CR aqueous solution (40 ppm), and 50 µl of a nanoparticle dispersion solution. The nanoparticle dispersion solution was prepared by dispersing 1 mg of CuO (N1) in 2 ml of distilled water. The resulting mixture was stirred in darkness for 25 minutes to achieve complete adsorption-desorption equilibrium. It was then placed in a custom-made photocatalytic chamber exposed to visible light from four Philips cool LED bulbs. The UV-visible spectrophotometer was used to record absorption spectrum of the reaction mixture at specific time intervals to track the degradation of CR by measuring its absorbance at 497 nm. Similarly, dispersion solution of N2, N3, and N4 were prepared and photocatalytic

degradation experiments were done in the presence of N2, N3, and N4 samples. CR model solution concentration was kept same as mentioned above for N2, N3, and N4 samples.

5.3.2. Results and discussions of CR degradation

Congo red degradation in the presence of N1, N2, N3, and N4 samples were performed in the presence of visible light and their UV-visible spectra was recorded for first 100 minutes. It is seen that N1 (*Figure 5.4(a)*) and N2 (*Figure 5.4(b)*) exhibit better CR removal than N3 (*Figure 5.4(c)*) and N4 (*Figure 5.4(d)*) as the absorption peak of CR at 497 nm wavelength gradually decreases in intensity. N1, N2, N3, and N4 exhibit 64.68%, 31.39%, 19.55%, and 9.29% CR degradation respectively (as shown in *Figure 5.5*). Also N1 degrades more CR than N2 in 100 min radiation time, which is evident from the reduced absorbance peak at 497 nm wavelength in *Figure 5.4(a,b).* So further investigation of CR degradation was carried on with N1 (CuO NPs) sample until maximum CR degradation was observed. CR degradation is not observed in the absence of photocatalyst (*Figure 5.6*).

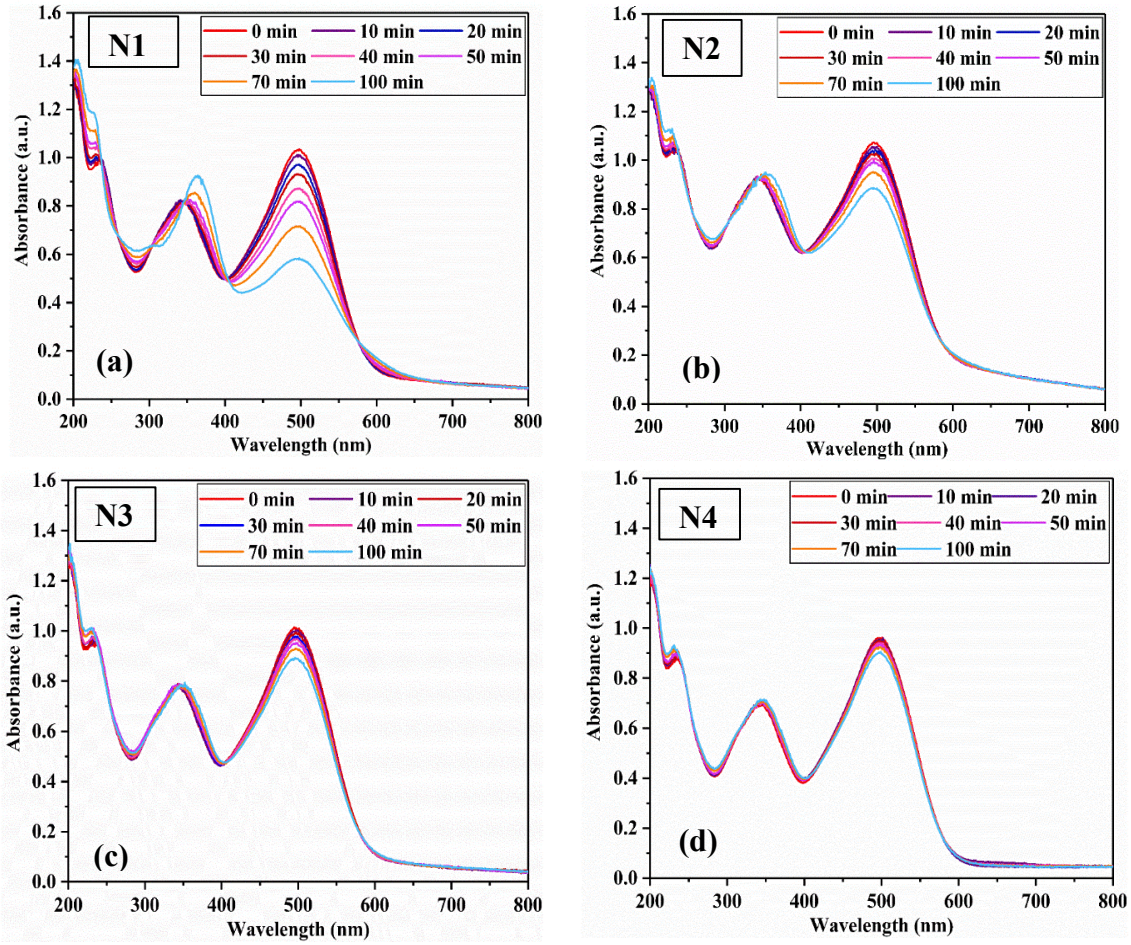

Figure 5.4 UV-visible spectra study of CR dye degradation recorded in the presence of N1, N2, N3, N4 catalyst upto 100 min visible light radiation

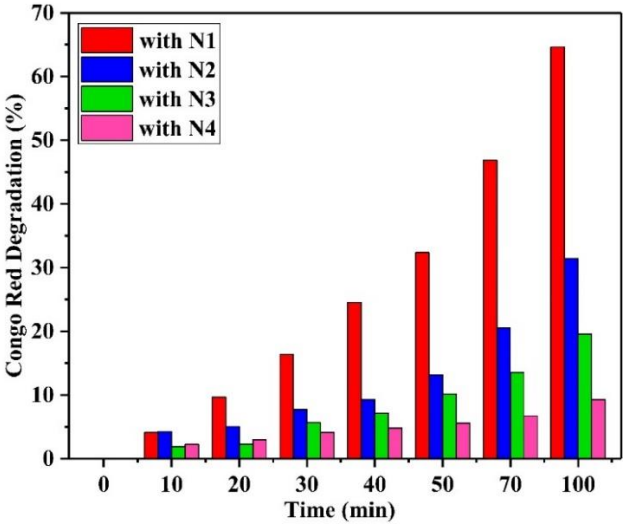

Figure 5.5 Percentage degradation of CR in the presence of N1, N2, N3 and N4 upto 100 min irradiation time

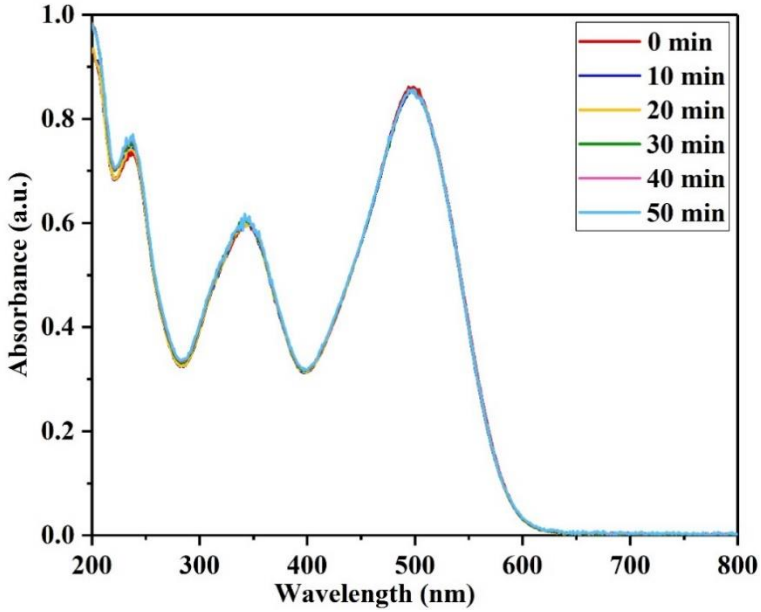

Figure 5.6 UV-visible spectra of CR dye recorded at different time points in the absence of catalyst

The photocatalytic degradation of Congo Red (CR) was accomplished under visible light luminance over the as-synthesized N1 sample. The UV-visible absorption spectrum of the CR degradation recorded at different time intervals is shown in *Figure 5.7*. It was observed that the main absorption peak of CR dye solution slowly subsides in the presence of CuO nanoparticles under visible radiation. The percent degradation of dye was calculated using *Eq (5.6)*,

$$\%\ Degradation = \left(\frac{C_0 - C}{C_0}\right) x\ 100 \qquad (5.6)$$

where C_0 is the initial dye concentration, C is the dye concentration at time t after exposure to visible irradiation. As seen from *Figure 5.8* CR exhibited a degradation of 96.79% at 180 minutes. *Table 5.1* shows the results of comparative assessment of CR degradation with CuO photocatalyst as reported in different literatures (Batool et al., 2019; Chimeno-Trinchet et al., 2019; Farbod et al., 2012; Pakzad et al., 2019; Vengatakrishnan et al., 2021).

Figure 5.9(a) presents the outcome of visible light irradiation on CR degradation with time, which shows the plots for experiments done both with and without catalyst (blank). CR degradation occurred only in the presence of photocatalyst in the reaction mixture. We tested the CR degradation data for zero, first, and second order kinetics fitting. It is best fitted with the first-order kinetics. *Figure 5.9(b)* shows the difference of –ln (C/C_0) with the irradiation time in accordance with the *Eq (5.7)* given below.

$$-ln\,(C/C_0) = k_{app}t \qquad (5.7)$$

Here, C is the concentration of CR at time t. C_0 is initial concentration of CR and k_{app} is the apparent rate constant. The rate constants found from the linear fit were 0.0046, 0.0022, 0.0012, 0.0005 min^{-1} for CR degradation in the presence of catalyst N1, N2, N3, and N4; and 0 min^{-1} for the sample in the absence of catalyst.

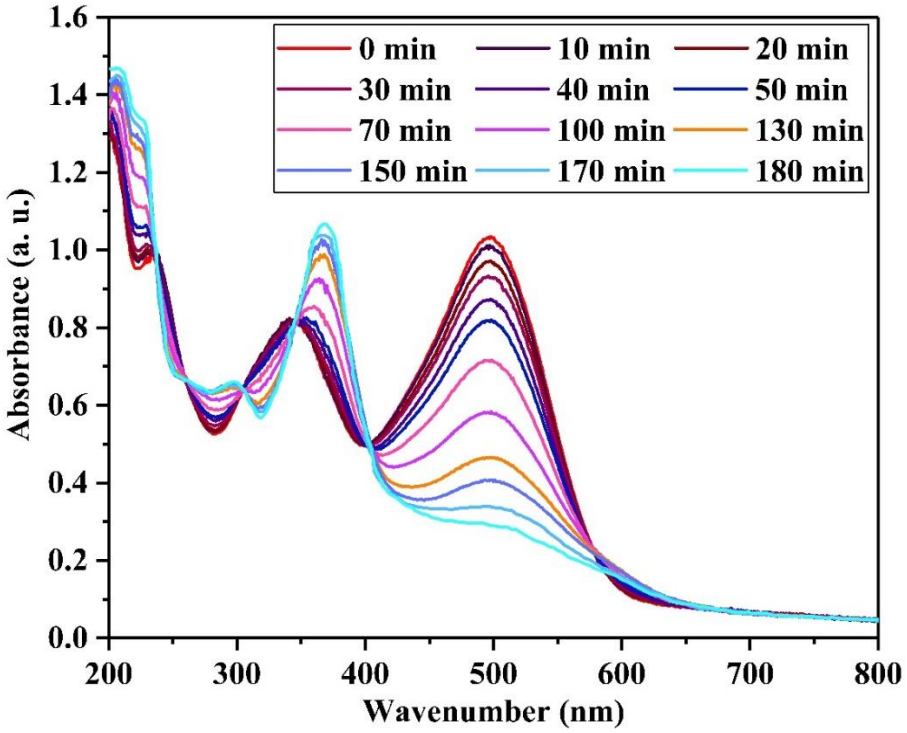

Figure 5.7 UV-visible spectra of CR dye recorded at different time points in the presence of N1 catalyst

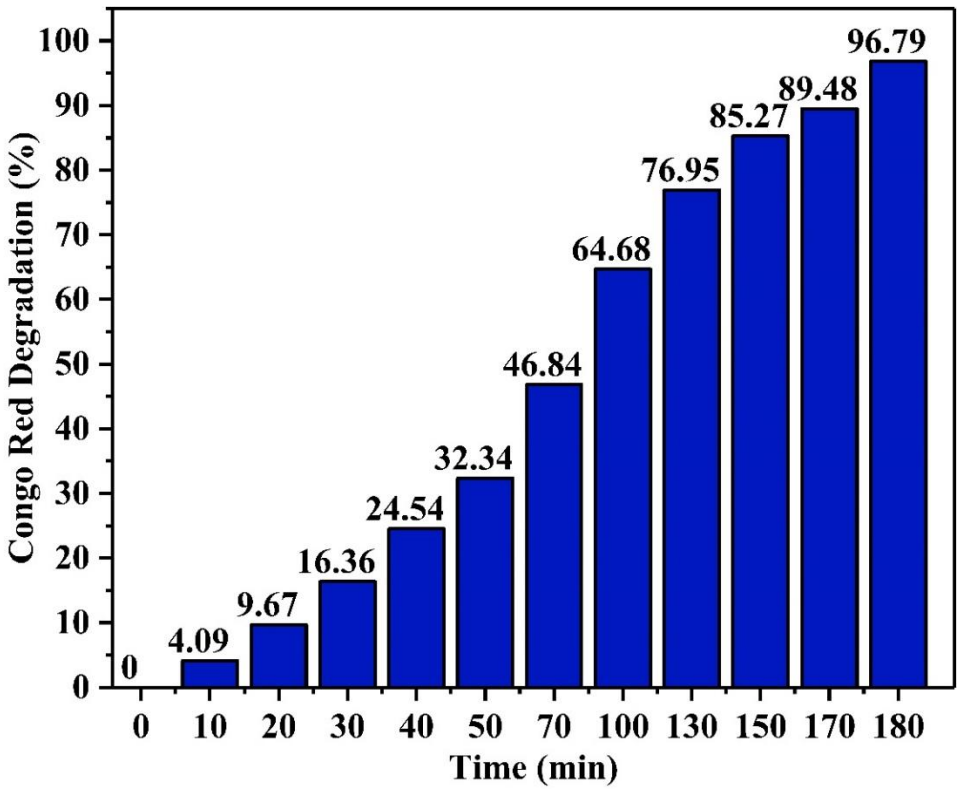

Figure 5.8 Percentage degradation of CR with N1 NPs

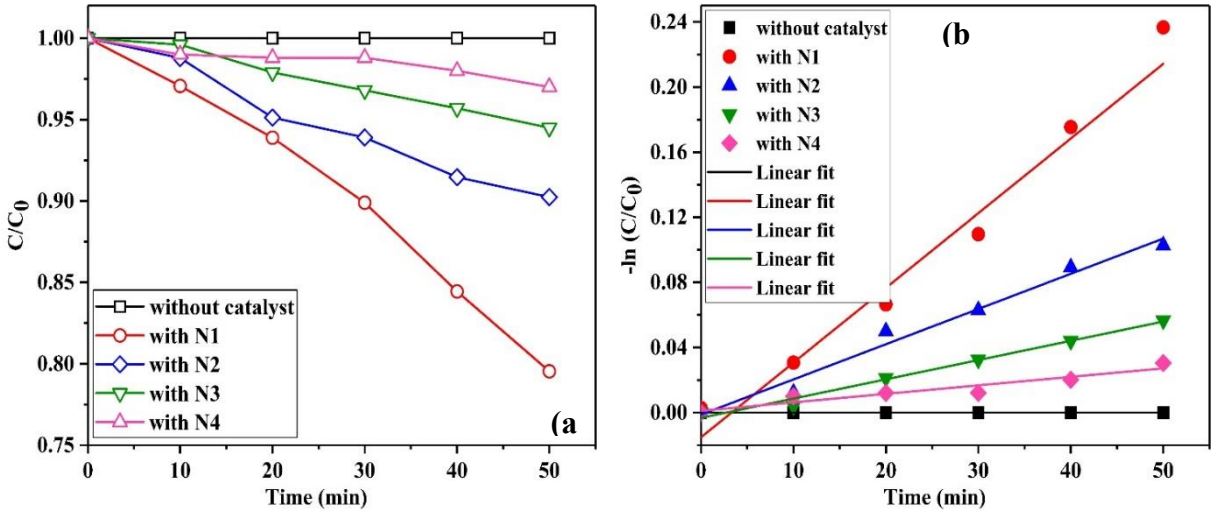

Figure 5.9 Kinetic study of photocatalytic performance of catalyst N1, N2, N3 and N4 with respect to CR dye degradation up to 50 min visible light irradiation

Table 5.1 Comparative assessment of Congo red degradation efficiency using CuO photocatalysts reported in different literatures

Photocatalyst	Synthesis method	Particle size	Bandgap energy (eV)	Pollutant model	Light source	Degradation (%)	Reaction Time	References
Cu_2O/CuO nanowires	Direct oxidation at 500°C	6.4 μm length, 95 nm diameter	-	20 mg/L	UV irradiation	75	210 min	Farbod et al., 2012
CuO nanospheres	*Euphorbia maculate* extract-mediated biosynthesis route	18 nm	-	10 mg/mL	UV	85	60 min	Pakzad et al., 2019
CuO nanospheres	Biosynthesis using aloe vera leaf extract	80-120 nm	-	10 mg/L	Visible light+H_2O_2	70	120 min	Batool et al., 2019
Alkyl-capped CuO nanospheres	Chemical precipitation	10±2 nm diameter	2.62	$2.5x10^{-4}$ M	Sunlight	95	1.5 days	Chimeno-Trinchet et al., 2019
CuO leaves	Precipitation method	-	3.05	500 mg/L	Solar	17.6	2 h	Vengatakrishnan et al., 2021
					UV	7.5	2 h	
CuO nanoparticles (N1 sample)	Precipitation	18.709±5.662 nm	1.93	40 mg/L	Visible light	96.79	180 min	This study

En dash (-) indicates data unavailable

5.4. Degradation of Methylene Blue

Methylene Blue (MB), a heteropolyaromatic dye (as shown in *Figure 5.10*), is used to colour cotton, coloured paper, wool, and paper stock dyeing. MB is toxic in nature. MB loaded effluent discharged into water bodies can cause eye burning, skin irritation, and problems in gastrointestinal tract. So it is essential to remediate the dye stuffed wastewater to save water and the environment (El-Sayed et al., 2022). MB has maximum absorption peak at 664 nm wavelength (Yin et al., 2021).

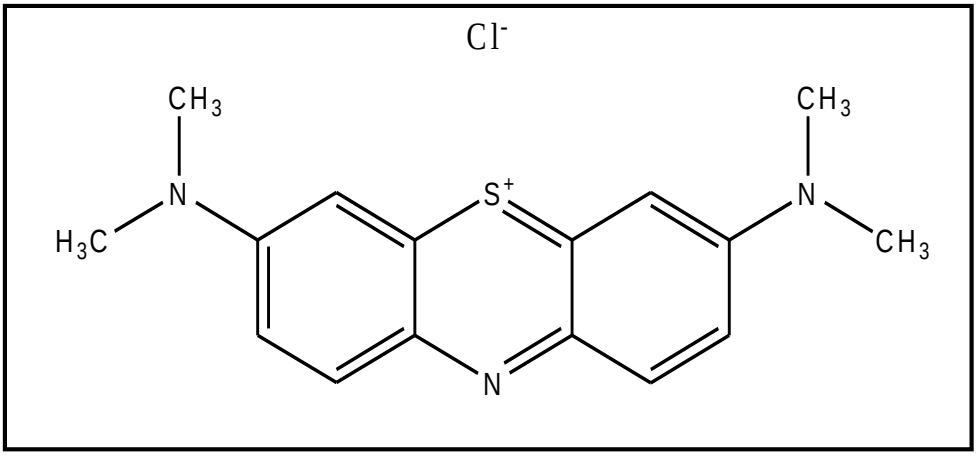

Figure 5.10 Chemical structure of Methylene Blue (El-Sayed et al., 2022)

5.4.1. Photocatalytic activity assessment

Dispersion NP solution was prepared by adding 1.6 mg as-synthesized nanoproduct to 3 ml distilled water and ultrasonicating it to achieve uniform dispersion. MB solution was prepared by adding 50 ml distilled water to 2 mg MB. 1 ml distilled water, 200 µL of 40 ppm MB aqueous solution and 100 µL of the NP dispersed solution were mixed together in 4 ml quartz mixture. This mixture was stirred in dark for 25 min. The degradation of MB dye through photocatalysis was conducted in a home-made photocatalytic chamber employing four Philips cool LED bulbs inside the chamber as visible light source.

Throughout the experiments, a consistent concentration of MB solution and catalyst (N1, N2, N3, and N4) was mixed in the reactor under continuous visible light irradiation. The degradation progress of MB was tracked by periodically subjecting the reaction mixture to UV-visible absorption spectrum study at a maximum wavelength of 664 nm.

5.4.2. Results and discussions of MB degradation

N1, N2, N3, and N4 samples underwent MB degradation under visible light, with their UV-visible spectra recorded for 120 minutes. N1 (*Figure 5.11(a)*) and N2 (*Figure 5.11(b)*) showed superior MB removal compared to N3 (*Figure 5.11(c)*) and N4 (*Figure 5.11(d)*), evident in the decreasing absorption peak at 664 nm. N1 exhibited the highest degradation (84.75%) followed by N2 (83.33%), N3 (82.08%), and N4 (81.22%) (as depicted in *Figure 5.12*). Further analysis revealed N1 outperformed N2 in degrading MB within 120 minutes of radiation, as seen in *Figure 5.11(a,b).* Subsequent investigation focused on N1 (CuO NPs) due to its maximum MB degradation. Notably, MB degrades at a very slow rate in the absence of catalyst under visible light illumination (*Figure 5.13*).

MB's photocatalytic degradation under visible light using the N1 sample was observed. *Figure 5.14* displays the UV-visible absorption spectrum over time, showing a gradual decrease in MB's main absorption peak in the presence of N1 (CuO) nanoparticles. *Figure 5.15* displays MB degradation of 98.09% over 200 minutes. *Table 5.2* compares MB degradation using CuO photocatalyst across various studies (Dulta et al., 2022; Farrouji et al., 2015; Mageshwari et al., 2015; Pakzad et al., 2019; Safa et al., 2015; Yugandhar et al., 2019; Zhu et al., 2013). Analysis revealed the degradation best fits zero-order kinetics, as depicted in *Figure 5.16*. The linear fit revealed rate constants of 0.0117, 0.0112, 0.0105, and 0.0104 min^{-1} for MB degradation in the presence of catalyst N1, N2, N3, and N4; and 0.0046 min^{-1} for the sample lacking catalyst.

The addition of catalytic material is realistic from an Industrial perspective. After its usage, the photocatalyst must be separated from the slurry and processed for reusability. Semiconductor catalysts such as TiO_2, $SrTiO_3$, ZnS, ZnO, CdS, $Ni/KTaO_3$, $CuCrO_2$ etc. have been used to remove pollutants from water. TiO2 has attracted a lot of interest in the field of photocatalysis because of its high catalytic efficiency, stability, and non-toxicity (Al-Nuaim et al., 2023). In our study we have investigated visible light irradiated i.e., solar light-driven photocatalysis for environmental remediation which can be tried in treatment of textile industry effluents for tackling global energy shortages and pollution. The photocatalytic water treatment studies take numerous elements into account, although they generally employ laboratory sites of simulated single pollutant wastewater, which nevertheless entails a high degree of complexity in comparison to genuine industrial or natural waste. Reactor design to enhance separation efficiency, photocatalyst optimization, and immobilization for recycling are all important aspects of furthering rational photocatalytic system development

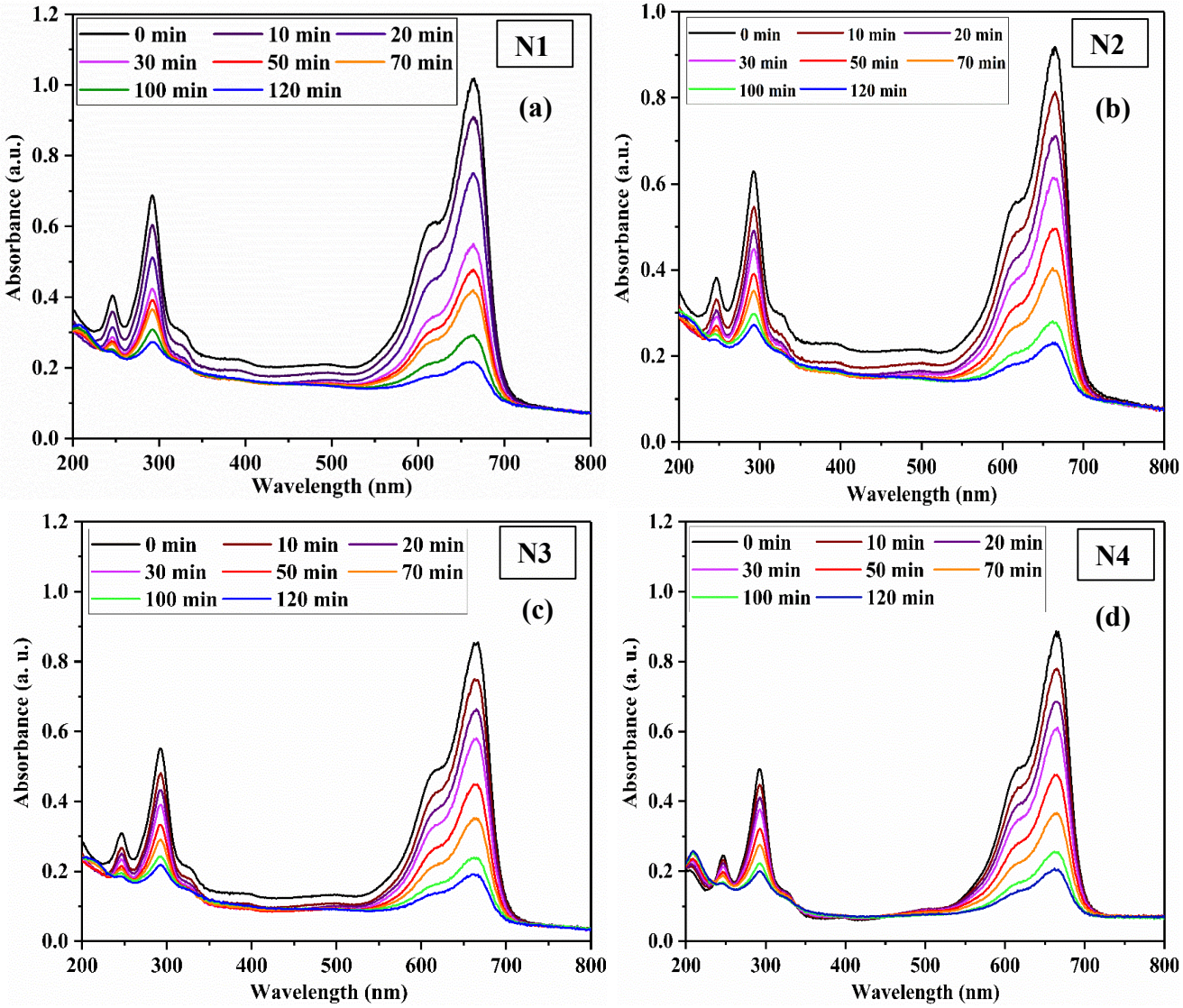

Figure 5.11 UV-visible spectra study of MB dye degradation recorded in the presence of (a) N1, (b) N2, (c) N3, and (d) N4 catalyst upto 120 min

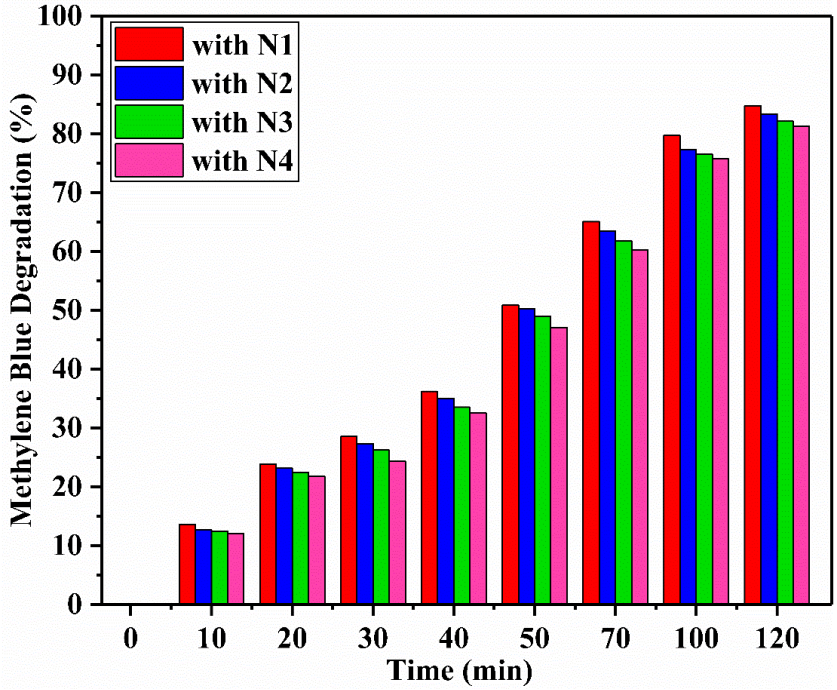

Figure 5.12 Percentage degradation of MB in the presence of N1, N2, N3, and N4 upto 120 min time period

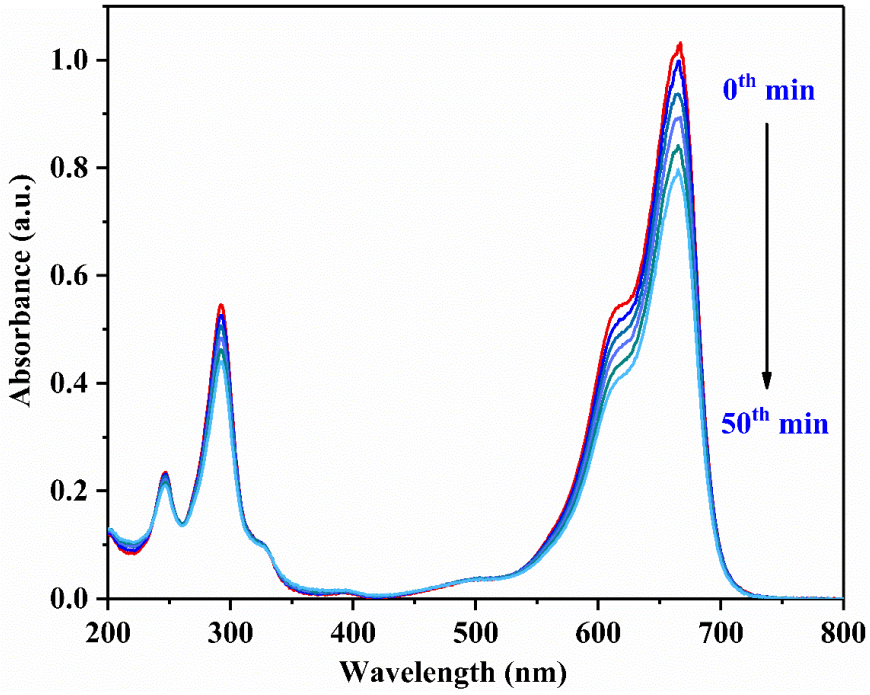

Figure 5.13 UV-visible spectra of MB dye recorded at different time points in the absence of catalyst

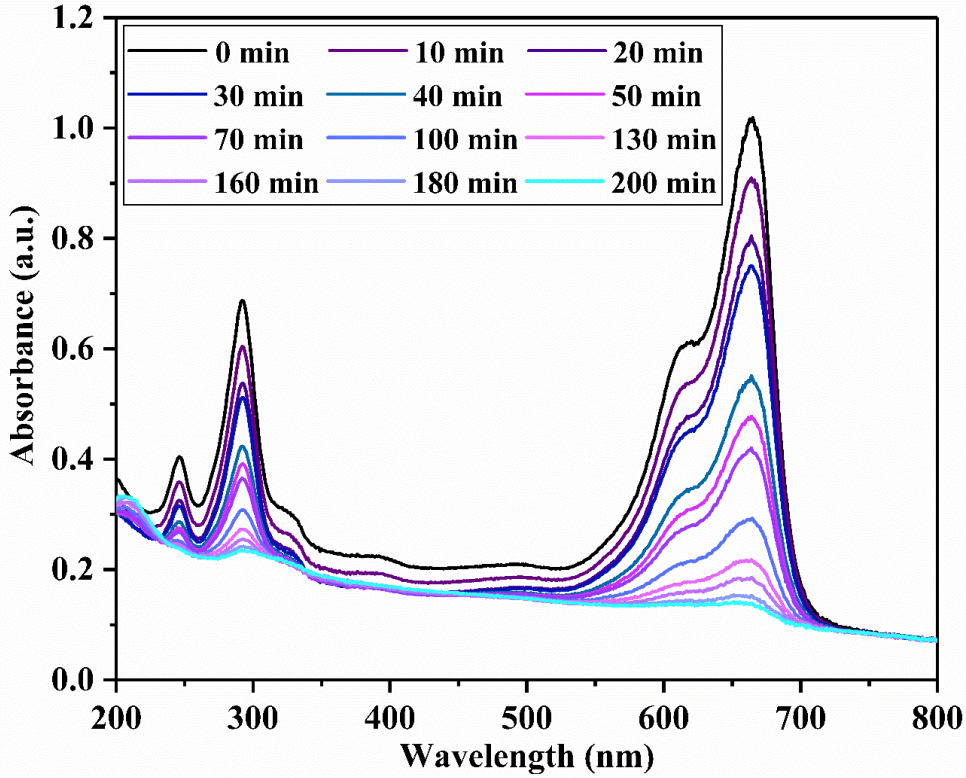

Figure 5.14 UV-visible spectra of MB dye recorded at different time points in the presence of N1 catalyst

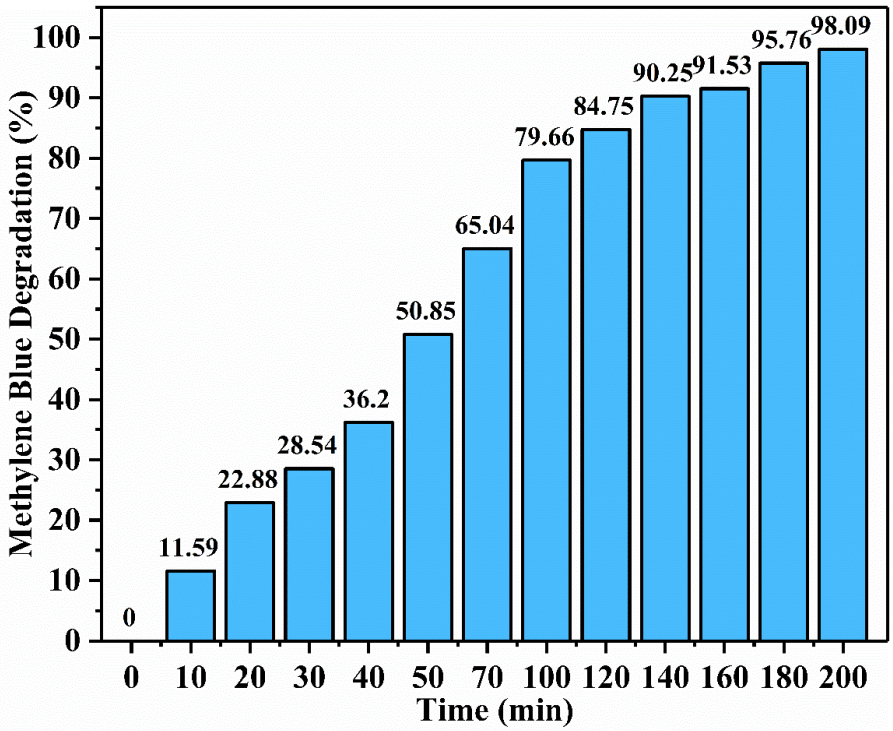

Figure 5.15 Percentage degradation of MB with N1 NPs

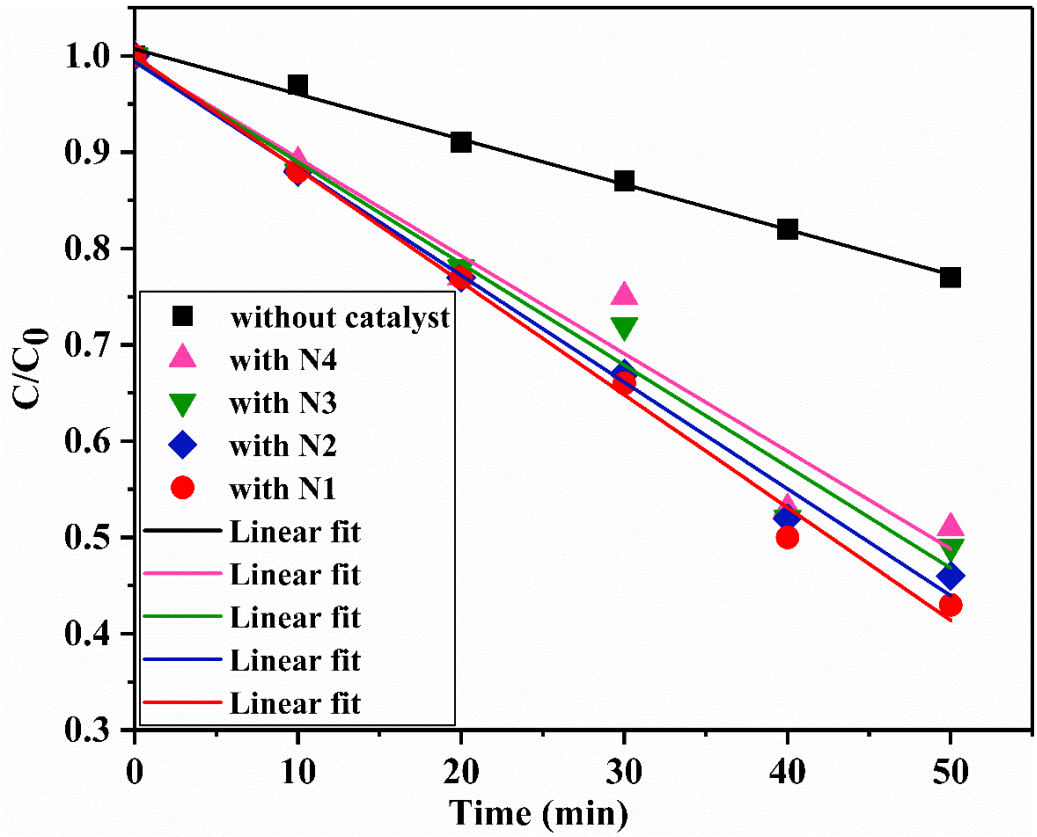

Figure 5.16 Kinetic study of photocatalytic performance of N1, N2, N3, and N4 catalysts with respect to MB degradation upto 50 min

Table 5.2 Comparative assessment of Methylene blue degradation efficiency using CuO photocatalysts reported in different studies

Photocatalyst	Synthesis method	Particle size	Bandgap energy (eV)	Model Pollutant concn.	Conditions of degradation	Degradation (%)	Reaction Time (min)	Ref.
CuO nanowires	Solution phase method	3-7 nm diameter, 8-30 nm length	-	10 mg/L	Visible light+ NaOCl	93.67	60	Farrouji et al., 2015
Flower shaped CuO microspheres with naosheets subunits	Reflux condensation method	-	1.59	15 ppm	UV light + H_2O_2	92	360	Mageshwari et al., 2015
CuO NPs	Biosynthesis with Rhizome extract of *Bergenia ciliata*	20 nm	-	20 ppm	Sunlight	92	135	Dulta et al., 2022
CuO Nanorods	Hydrothermal method	-	-	20 mg/L	Visible light+ H_2O_2	100	180	Safa et al., 2015
CuO nanospheres	Biosynthesis with *Syzygium alternifolium* leaf extract	54.5 nm	-	5 mg/L	Visible light	83.1	320	Yugandhar et al., 2019
CuO nanosheets	Hydrothermal method	400 nm width	-	$6x10^{-5}$ mole/L	Visible light+ H_2O_2	96.5	180	Zhu et al., 2013
CuO nanospheres	*Euphorbia maculate* extract-mediated biosynthesis route	18 nm	-	10 mg/mL	UV	96	60	Pakzad et al., 2019
CuO NPs (N1)	Precipitation	18.709±5.662	1.93	40 mg/L	Visible light	98.09	200	Present study

En dash (-) indicates data unavailable

5.5 . Plausible photocatalytic mechanism

This section demonstrates a plausible photocatalytic mechanism for dye degradation. *Figure 5.17* displays the schematic diagram of the possible photocatalytic mechanism of the dye degradation (here, CR or MB). In the presence of visible light source, the CuO photocatalyst generates substantial amount of holes (h^+) and electrons (e^-) in the valence band (VB) and conduction band (CB) respectively. The dye can be oxidized by VB's h^+. Meanwhile, the photo-generated e^- reduces the oxygen molecule present in the reaction system. This reduction results in superoxide radical ($O_2^{\cdot -}$) formation, which can further produce hydroxyl radical ($OH^{\cdot}$). As formed $OH^{\cdot}$ radical takes part in the dye degradation process resulting in the formation of CO_2, H_2O, and other less harmful by-products.

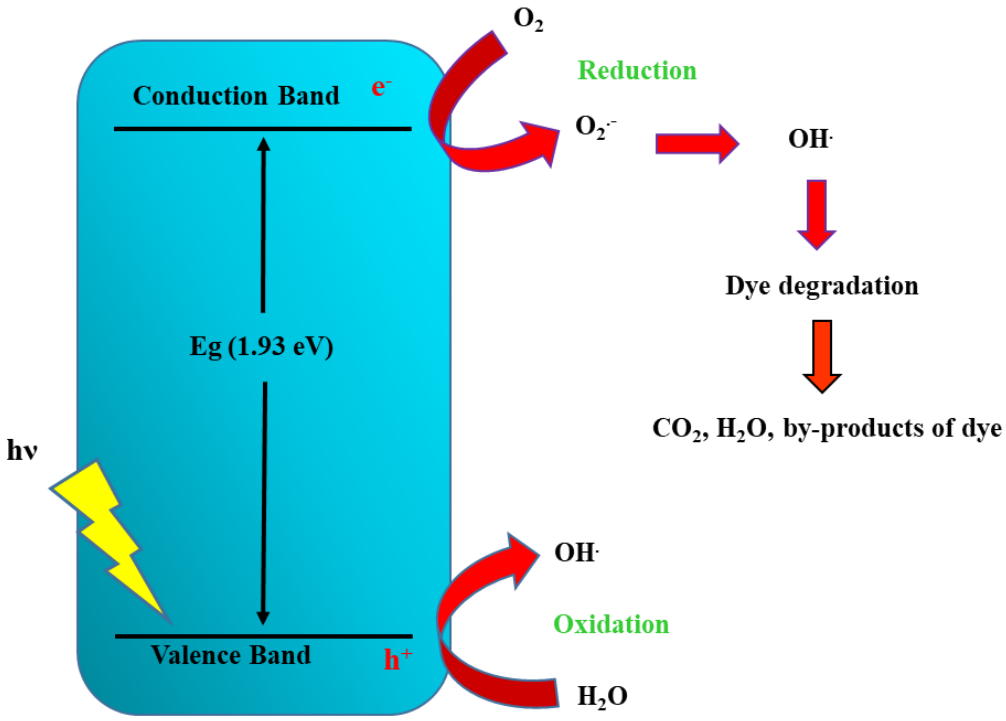

Figure 5.17 Schematic diagram of the plausible photocatalytic mechanism

5.6 . Understanding the photocatalytic behaviour of recovered nanoproducts

We can conclude from section 5.3 and 5.4 that N1 is a better photocatalyst than N2, N3, and N4 nanoproducts as it shows better degradation of dye (CR, MB) in the presence of visible light. *Table 5.3* summarizes the values of different parameters obtained from the characterization results of the synthesized nanoproducts N1, N2, N3, and N4. The spherical morphology of N1 and N2 provide higher surface area for photocatalytic reactions to occur compared to the sheet and microsphere morphology of N3 and N4. The average particle size crystallite size of N1 is less than that of N2 which means more reaction sites are available in N1 than in N2 for dye degradation reactions to occur. This increased surface area allows organic dye molecules to access the photocatalytic active sites more effectively, boosting the reactivity and dye adsorption (Marathey et al., 2019). The optical band gap energy of N1 and N2 is higher than that of N3 and N4, which is due to occurrence of smaller sized NPs in N1 and N2 than N3 and N4 (Liu et al., 2006). The increased BET surface area and porosity of N1 compared to N2 contribute to increased surface oxygen vacancies, thus improving visible light absorption. These oxygen vacancies act as active sites for photocatalytic reactions causing increased photocatalytic activity of CuO NPs under visible light irradiation (Wang et al., 2016). N1 contains more oxygen vacancies than N2 i.e. 39.88% in N1 and 31.34% in N2. Higher oxygen vacancies serve as electron-hole acceptors in photocatalytic reactions, which assist in capturing photo-induced electrons from adsorbed oxygen, generating superoxide radical anions, which in turn generate more hydroxyl radicals, thus improving the photocatalytic capabilities of N1 (Marathey et al., 2019).

Table 5.3 Characterization results summarized for N1, N2, N3, and N4 samples

Sample name	Phase obtained	Average crystallite size (nm)	Average particle size (nm) [from TEM]	Bandgap energy (eV)	BET surface area ($m^2 g^{-1}$)	Pore volume ($cm^3 g^{-1}$)	$O_{vacancy}$ (%) [from XPS]
N1	CuO nanospheres	18.049	18.709±5.662	1.93	32.40	0.1201	39.88
N2	CuO nanospheres	19.236	19.973±6.036	1.97	28	0.1018	31.34
N3	CuO nanosheets	24.394	55.997±16.892	1.86	-	-	-
N4	CuO microspheres	28.772	975.672±304.281	1.48	-	-	-

En dash (-) indicates not analysed for specific sample

5.7 . Conclusions

In this chapter a detailed photocatalytic activity investigation of the recovered nanoproducts is reported. Moreover, a comparative study was done to conclude that N1 nanoproduct that we recovered from the leach liquor in chapter 4 can find potential application as a photocatalyst to treat wastewater generated from textile industries. The major outcomes of this chapter are given below:

- N1 exhibited better photocatalytic property than N2, N3, and N4.
- Under visible light irradiation N1 NPs exhibited 96.79% Congo Red degradation in 180 min.
- Also Methylene Blue showed a degradation of 98.09% in the presence of N1 photocatalyst under 200 min visible light irradiation.
- The higher photocatalytic activity of CuO NPs of N1 sample can be ascribed to:

i. Lower particle size and irregular morphologies which provide higher surface area, hence increasing the number of active sites, resulting in higher reactivity and increased adsorption of dye

ii. difference in the oxygen defects/vacancy between N1 and other samples

iii. lower crystallite size

iv. higher BET surface area of N1 which contribute to the increase of surface oxygen vacancies, which improve visible light absorption and act as active sites for photocatalytic reactions leading to enhancement of photocatalytic activity of CuO NPs under visible light irradiation

v. larger pore volume, leading to higher porosity provides transmission paths for organic dye molecules, which can sufficiently access the photocatalytic active sites of N1.